On the feasibility of Laser-Induced Incandescence technique for TiO2 nanoparticles analysis

J Yi, Christopher Betrancourt, Nasser Darabiha, Benedetta Franzelli

On the feasibility of Laser-Induced Incandescence technique for TiO_2 nanoparticles analysis

J. Yi[1*], C. Betrancourt[1], N. Darabiha[1], B. Franzelli[1]

[1]Université Paris-Saclay, CNRS, CentraleSupélec, Laboratoire EM2C, 91190, Gif-sur-Yvette, France.

Abstract

This work-in-progress study aims to develop a method to verify the possibility of measuring the Laser-Induced Incandescence (LII) signal from TiO_2 nanoparticles. For this, the optical system for LII was first validated on flame-generated soot particles. Then, spectrally-resolved measurements of laser-induced emission of TiO_2 nanoparticle-laden aerosol were performed. At 355 nm laser wavelength, the laser-induced emission spectrum presents a response to laser fluence and detection gate delay typical of the black-body radiation, i.e., dependent on the particle temperature. It is concluded that laser-induced incandescence is possible for non-carbonaceous TiO_2 nanoparticles.

Introduction

Turbulent flame synthesis is today considered as a promising technique for the large-scale production of nanoparticles with high purity at a reduced cost [1]. In most applications, the unique properties of produced nanoparticles (e.g., increased catalytic activity, change in optical property, lower reaction sintering temperatures [1]) closely rely on their nano-size, so there is a crucial need to understand the processes underlying nanoparticles production in turbulent flames. For this, the generalization of in situ experimental techniques classically used to characterize soot production in flames to non-carbonaceous nanoparticles, such as titanium dioxide (TiO_2) [2], can be considered as a promising opportunity to gain knowledge on flame synthesis technology.

Among them, the laser-induced incandescence (LII) technique is classically used to obtain spatially-resolved information on soot volume fraction and primary particle size in flames [3]. This technique consists of heating the particles to a high temperature using a pulse laser. Subsequently to the heating phase, the particles cool down and emit thermal radiation to the surrounding environment. The signal intensity is proportional to particle volume fraction. The temporal signal decay is related to the particle size since large particles tend to cool down slower than small particles. Even if this technique is well-established for soot particles, its application to nanomaterials, particularly non-carbonaceous particles [4–6], presents specific difficulties in terms of their different optical characteristics compared to soot.

One important property for LII mechanisms is the refractive index m_λ [7]. The refractive index $m_\lambda = n_\lambda - ik_\lambda$ is a wavelength-dependent optical property describing the scattering characteristic (opacity) with the real part n_λ and the light-absorbing capacity (color strength) with the imaginary part k_λ [8]. This value is directly related to the amount of particles' laser energy absorption and the LII signal emission [9,10], so it is an important factor for the particle heating and the LII emission process. The typical values of $E(m_\lambda)$ for different types of soot and TiO_2 nanoparticles are shown in Fig.1. $E(m_\lambda)$ can vary on the particle size [11], phase [12], and other process variables in their fabrication [13,14]. The TiO_2 nanoparticles generally show very low $E(m_\lambda)$ compared to those of soot in the visible range (Fig.1).

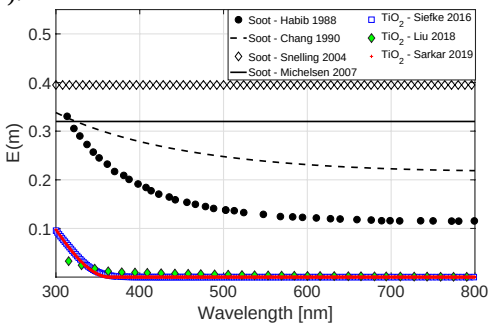

Figure 1: The spectral dependence of absorption function $E(m_\lambda)$, for soot particles generated by propane premixed flames (Habib [14] and Chang [15]) and typical values for soot modeling (Snelling and Michelsen [16]) for TiO_2 particles from Siefke [17], Liu [18] and Sarkar [19].

Therefore, the first difficulty in extending LII from near-grey-body soot to non-carbonaceous nanoparticles is the low absorption function $E(m_\lambda)$ of TiO_2 in the VIS-IR wavelength range. In the LII process, the particles have to absorb the incident laser beam to be heated to a higher temperature. Due to the low values of $E(m_\lambda)$ for TiO_2, particle heating by excitation laser whose wavelength is above UV range is expected to be challenging. In specific, classically used VIS-IR range light for particle heating could fail to heat the particles efficiently, as mentioned in the case of alumina in [20].

The second difficulty concerns the detection of laser-induced emission. A low signal is expected with the negligible $E(m_\lambda)$ in the LII detection wavelength range

* Corresponding author: junghwa.yi@centralesupelec.fr

(400-700 nm)[9,10]. Furthermore, the possible overlap of atomic and molecular emissions from various sources (excited-state emission from gas, electronically excited vaporized species, chemiluminescence, particle photoluminescence, incandescence) makes it even more difficult to distinguish the nature of the signal, as detailed in [21].

Finally, other physicochemical properties that show different aspects than those from carbonaceous particles add more complexities in the LII modeling for particle sizing. For example, the LII models should be tuned for lower sublimation temperatures for non-carbonaceous materials compared to soot particles [21]. The melting process [10] can influence particle heating and cooling rates because of differences in physical properties between solid and liquid states.

In the pioneering works of the CNR-ICMATE group [6,22,23], the laser-induced emission of flame-synthesized TiO_2 has been investigated. They conduct spectral measurements on flame-generated TiO_2 nanoparticles deposited on a filter and directly on the flame spray. The fourth harmonic (266 nm) of a pulsed Nd:YAG laser was used to heat the particles. The spectral emission was collected using a spectrograph with an intensified charged coupled device (ICCD) camera by delayed detection (longer than 50 ns) to delete fluorescence. The emissivity of TiO_2 was derived from extinction measurement. In the experimental configurations retained by the CNR-ICMATE group, two technical issues may occur: the detected signal may be affected by the use of a sampling glass filter [23] and by the possible existence of carbon coating around the considered flame-synthesized TiO_2 nanoparticles [24].

To circumvent the possible issues of CNR-ICMATE group works [6,22,23], in the present work commercial engineered TiO_2 nanoparticles with high purity are dispersed in aerosol form, instead of considering a glass filter sampling of flame-synthesized TiO_2 nanoparticles. This new contribution will allow to further confirm or disprove the conclusions from the CNR-ICMATE group works [6,22,23].

The paper first reviews the LII theory derived from Plank's law under various laser fluences and detection gates. Two experimental set-ups for investigating flame-generated soot and TiO_2 nanoparticle aerosol are presented in three parts: particle generation, laser excitation, and signal collection. Spectrally-resolved LII-emissions of soot particles in flames are measured to obtain a reference experimental behavior with laser fluence and detection gate delays in addition to the theoretical formulation. Then, spectrally-resolved laser-induced emission measurements from pure TiO_2 particles are performed. The results are compared to the spectral behavior of LII soot measurements to verify the LII-like nature of signal emission from TiO_2 nanoparticles.

1. LII theory: effect of laser fluence and detection gate delay

Numerical models describe particle heating and cooling mechanisms, including conduction, radiation, and sublimation. The governing heat and mass transfer equations during the LII process can be written as:

$$\frac{\pi d_p^3(t)}{6}\rho c_p\frac{dT_p}{dt} = \dot{q}_{abs} - \dot{q}_{cond} - \dot{q}_{sub} - \dot{q}_{rad} \quad (1)$$

$$\frac{dm_p}{dt} = -\dot{m}_{sub} \quad (2)$$

where d_p, m_p and T_p are particle diameter, mass, and temperature; ρ and c_p are the density and the specific heat of the particle; $\dot{q}_{abs}$ is the laser absorption; and $\dot{q}_{cond}, \dot{q}_{sub}$, and $\dot{q}_{rad}$ are the heat losses due to conduction, sublimation, and radiation of particle. $\dot{m}_{sub}$ is the mass-loss rate from the particle surface during the sublimation process.

Nanoparticles' laser energy absorption rate in the Rayleigh regime ($\pi d_p/\lambda_{ex} << 1$) is given by

$$\dot{q}_{abs}(t) = \frac{\pi^2 d_p^3}{\lambda_{ex}} E\left(m_{\lambda_{ex}}\right) F q(t) \quad (3)$$

where λ_{ex} is the excitation laser wavelength, F is the laser fluence (joules per unit area), $q(t)$ is the temporal profile of the laser pulse, and $E(m_\lambda)$ is the absorption function of complex refractive index m_λ:

$$E(m_\lambda) = -Im\left(\frac{m_\lambda^2 - 1}{m_\lambda^2 + 2}\right) \quad (4)$$

As already stated in the introduction, it can be concluded from Eq. (3) that the nanoparticle absorption rate and, consequently, its heating through laser energy strongly depend on $E\left(m_{\lambda_{ex}}\right)$.Therefore, efficient heating of TiO_2 nanoparticles may be challenging due to small values of $E\left(m_{\lambda_{ex}}\right)$ observed in Fig. 1.

The radiation emitted by one particle at the thermodynamic equilibrium can be derived using the monochromatic emittance $I_{bb}(\lambda_{em},\ T)$ of Plank's law,

$$I_{bb}(\lambda_{em}, T) = \frac{2\pi hc^2}{\lambda_{em}^5}\left[\exp\left(\frac{hc}{\lambda_{em}k_B T}\right) - 1\right]^{-1} \quad (5)$$

where h is the Planck constant, k_B is the Boltzmann constant, c is the speed of the light, and λ_{em} is the emission wavelength.

The monochromatic LII signal at emission wavelength λ_{em} is expressed using Plank's law:

$$S_{LII}\left(\lambda_{em}, T_p(t)\right) = 4\frac{\pi^2 d_p^3}{\lambda_{em}} E\left(m_{\lambda_{em}}\right) I_{bb}\left(\lambda_{em}, T_p(t)\right)$$

$$= 4\frac{\pi^2 d_p^3}{\lambda_{em}} E\left(m_{\lambda_{em}}\right)\frac{2\pi hc^2}{\lambda_{em}^5}\left[\exp\left(\frac{hc}{\lambda_{em}k_B T_p(t)}\right) - 1\right]^{-1} \quad (6)$$

The expression of the LII signal underlines its dependences with emission wavelength, temperature and time, as already pointed out in the introduction. As discussed in the introduction, the emission signal from TiO_2 nanoparticles may be difficult to be measured since it is expected to be low when looking at the $E\left(m_{\lambda_{em}}\right)$ values in Fig. 1.

Plank spectra $I_{bb}(\lambda_{em}, T)$ of Eq. (5) are presented in Fig. 2 for different particle temperatures. These spectra present a substantial variation of intensity in the visible-IR wavelength range. The maximum intensity of the spectral profile shifts towards smaller wavelengths when considering higher temperature values. This typical black-body radiation behavior, called Wien's

displacement law, is used in this work as a first LII signal indicator of particles' laser-induced signal.

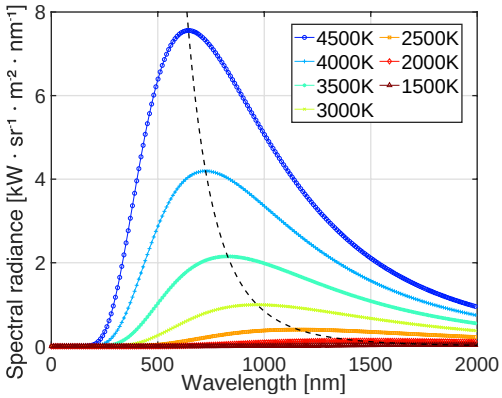

Figure 2: Spectral radiance of black-body for various temperatures. The dotted line corresponds to Wien's displacement law.

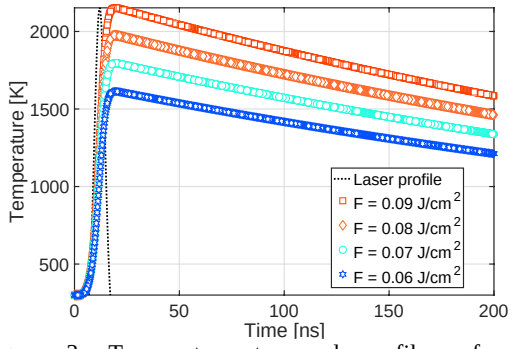

Figure 3: Temperature temporal profiles of particles experiencing LII for various laser fluences at 1064 nm. Results from numerical simulations of monodispersed spherical soot particles in an ambient environment (d_p=40 nm, $E(m_\lambda)$=0.4, thermal accommodation coefficient α=0.37). The dotted line represents the laser profile considered for the simulation.

Figure 3 illustrates the temporal temperature profile of the LII signal simulated for various fluences using an in-house code based on the signal modeling description of LIIsim [25] and the conduction model developed by [26].

From this temporal profile of the particle temperature, two important aspects of the LII behavior are observed:

(1) The particle temperature increases by increasing the input laser fluence F conforming to Eq. (3).

(2) For a given fluence, the temperature decreases with time due to the particle cooling. This temperature decreasing will induce a shift of the LII spectral profile, as shown for black-body radiation in Fig. 2.

Accordingly, by measuring the induced spectrum as a function of laser fluence F and detection gate delay τ_d, it is possible to verify the incandescent nature of the laser-induced signal of TiO_2 nanoparticles if the black-body behavior is retrieved.

2. Experimental set-up

The experimental set-up in Fig. 4 is composed of three elements: the system for particle generation, the laser excitation, and the signal collection.

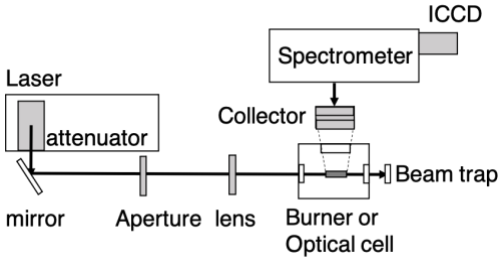

Figure 4: Schematic of the experimental set-up to investigate laser-induced emission from flame-generated soot particles (section 3.1) using a pulse laser YAG at 1064 nm with a top-hat spatial profile and from TiO_2 nanoparticle-laden aerosol (section 3.2) without aperture and lens using a pulse laser YAG at 355 nm with a Gaussian spatial profile.

2.1 Particles generation: soot particles in flames and dispersed TiO_2 nanoparticles

Two different particle generation systems are considered here when performing the measurements on soot or TiO_2 nanoparticles.

A steady non-premixed methane flame stabilized on a co-flow burner designed at Yale University [27] is used to generate the soot particles. The burner consists of a stainless-steel inner tube for methane injection with a diameter of 3.9 mm and a wall thickness of 0.5 mm. It is surrounded by a concentric air co-flow of a diameter of 76 mm. The air passes through 3 mm glass beads and two layers of honeycomb sections (cell size of 0.8 mm) to obtain uniform straightened flow without flow disturbances.

The methane flow has a bulk velocity of 28 cm/s (0.189 slm), and air co-flow has a bulk velocity of 15 cm/s (27.8 slm). Both flowrates are controlled using mass flow controllers (Bronkhorst EL-FLOW). These conditions result in a visible flame of 40 mm height, as shown in Fig. 5 (left).

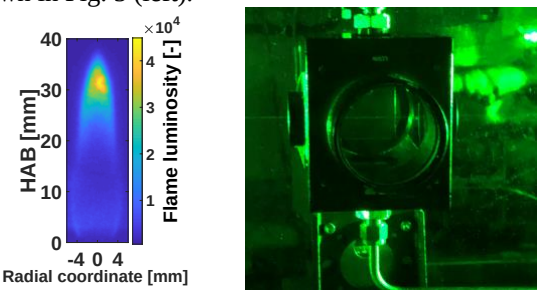

Figure 5: (left) Flame luminosity image (by ICCD camera) of the non-premixed methane co-flow flame considered here for the soot particle case. (right) Picture of the optically-accessible cell for LII system on TiO_2 nanoparticle-laden aerosol.

The LII measurements have been conducted at the peak soot volume fraction on mature soot (Height Above the Burner HAB =31 mm).

For TiO_2 nanoparticle-laden aerosol, the laser-induced emission measurements are conducted considering nanoparticle aerosol dispersion in a non-reactive ambient environment. Commercial TiO_2 nanoparticles (nanografi, NG04SO3508 Rutile, purity: 99.99+ %) are transported by air (16.67 slm, 9.8 m/s, and Re ~ 3700) in a 1L flask volume placed inside an

ultrasonic water bath (360W). The solid-gas flow passes through a 1L buffer volume to have a homogenous distribution of particles. Finally, the solid aerosol is dispersed in an optically-accessible cell (6 cm cube), with 1-inch windows for laser path and a 2-inch window for detection, as presented in Fig.5 (right). The flow is evacuated out to the top hood. The TiO_2 nanoparticles are then irradiated by a laser pulse inside the cell, and the corresponding signal is collected through the perpendicular window by the collector.

Since the dispersion of the TiO_2 powder is time-variant, the particles inside the first flask volume are refilled after each series of measurements (m_g= 150 mg of particles). It has been verified that a variation on the initial quantity of solid nanoparticles m_g does not affect the particle's spectral behavior.

The pure TiO_2 nanoparticle-laden aerosol is used to avoid any effect of undesired carbonaceous coating in the measured signal, which is commonly mentioned in the synthesis of pure metal-oxide nanoparticles via flame spray pyrolysis [24,28]. By using air to disperse particles in measurement volume, the obtained laser-induced emission is free of interferences like laser-induced fluorescence of flame gaseous species or possible laser interaction with the sampling glass filter [23].

2.2 Laser excitation

Two laser excitation strategies have been developed to minimize the interferences of signals and maximize laser absorption of particles.

For flame-generated soot particles, an Nd: YAG laser beam (Continuum, Surelite 3) of 1064 nm wavelength with a repetition rate of 10 Hz and 5 ns FWHM pulse duration is used. The beam presents a top-hat 0.7×0.8 mm^2 energy distribution by the rectangular-shaped aperture. The top-hat laser is then relay-imaged to the vertical centerline of the flame. The laser energy can be controlled using an attenuator consisting of a half-wave plate and a polarizing beam splitter. For soot particles in flames, the fundamental harmonic is preferred here to avoid the parasite signal from laser-induced fluorescence of polycyclic aromatic hydrocarbons (PAH) and soot light scattering [9].

For TiO_2 nanoparticles, the particles in the control volume are heated by a pulsed 355 nm Nd: YAG laser (Quantel, Q-smart 450), with a repetition rate of 10 Hz and a 5 ns FWHM pulse duration. This beam is a spatially Gaussian distribution with a diameter of 6.5 mm. The laser pulse is headed directly to the optical cell by a mirror, without any other aperture or lens. The laser energy is controlled via an attenuator adapted for 355 nm.

The laser wavelength of 355 nm has been chosen here to ensure that TiO_2 nanoparticles absorb the laser beam and so as to be heated (Fig.1).

Table 1: Summary of the experimental set-ups for flame-generated soot particles and TiO_2 aerosol.

Purpose	Flame-generated soot	TiO_2 aerosol
Laser	Surelite 3	Q-smart 450
Wavelength	1064 nm	355 nm
Pulse duration (FWHM)	5 ns	5 ns
Beam profile	Top-hat (Rectangular 0.7 mm by 0.8 mm)	Gaussian (Round 6.5 mm)
Gate width	5 ns	20 ns

2.3 Signal collection

For both soot and TiO_2 diagnostic systems, the same collector is used to collect the induced signal at 90° of the laser path. The collector is constituted of two achromatic lenses with a magnification factor of 2. The collector is connected to a spectrometer (Princeton Instruments, HRS-500) with a grating groove density of 150 groove/mm, and an ICCD camera (Princeton Instruments, PI-MAX 4, Gen III intensifiers HBf) by the mean of a multimode optical fiber (Thorlabs, FG365UEC) with a core diameter of 365 μm.

For the prompt measurement of the TiO_2 system, a 532 nm notch filter is used in front of the collector to reject the 532nm residual of the laser. For flame-generated soot particles, the measurement volume is 0.4 mm^3 cuboid. For the TiO_2 dispersion diagnostic system, the measurement volume is a cylinder of 6.5 mm.

The ICCD camera is operated with a gate width adapted for each system (summarized in Table 1). In the case of TIO_2, bigger gate width is used to improve the signal-to-noise ratio. With the on-CCD accumulation function of the ICCD camera, over 500 single shots are acquired and then averaged for each measurement in both cases. Different gate delays (τ_d = 0 – 1000 ns) are considered for the temporal acquisition of laser-induced emission.

The detection system is calibrated using a tungsten filament lamp for signal intensity and a mercury lamp for wavelength.

3. Laser-induced signal characterization

In this section, the typical laser-induced incandescence signal of soot as a function of laser fluence F and gate delay τ_d is presented and analyzed based on LII theory. Then the same studies are performed on laser-induced emission of pure TiO_2 particles.

3.1 Laser-induced incandescence behavior of soot particles in flames irradiated at 1064 nm

Figure 6 shows the prompt (τ_d = 0) emission spectra of soot particles under various laser fluences F for an excitation laser wavelength of 1064 nm. The spectra are fitted by Eq. (6), considering a constant absorption function ($E(m_\lambda)$ =0.4) to determine the heated soot temperature. The LII signals exhibit continuous spectra in the visible wavelength range, with the signals decreasing to low levels for small wavelengths. When increasing the laser fluence, the curves move towards short wavelengths, indicating increased particle heating temperatures. This behavior conforms to the LII theory presented in section 1. Furthermore, it can be observed that at high fluences, the LII spectra show distinct peaks at 516 nm (C_2 swan band).

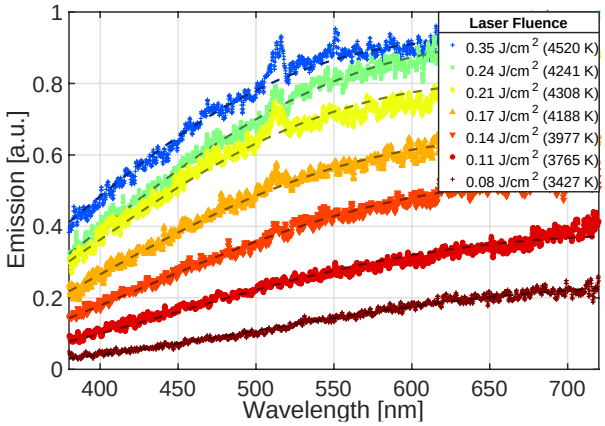

Figure 6: Emission spectra of laser-induced emissions of soot particles under various laser fluences F at prompt. The temperature inside the parenthesis is fitted using Eq. (6), with constant $E(m_\lambda) = 0.4$. All curves are normalized by the maximum value obtained for fluence F= 0.35 J/cm^2.

By changing the gate delay τ_d with respect to the prompt timing for a given fluence (F = 0.3 J/cm^2), this black-body-like tendency is again confirmed in Fig. 7. By increasing the detection gate delay τ_d, the spectra peak shifts to big wavelengths due to the soot temperature decrease.

The spectral trends with various laser fluences and detection gate delays confirm the LII nature of the measured laser-induced emission from soot particles. These trends validate the experimental protocol retained in this work to demonstrate the possible induced incandescence behavior of TiO_2 nanoparticles.

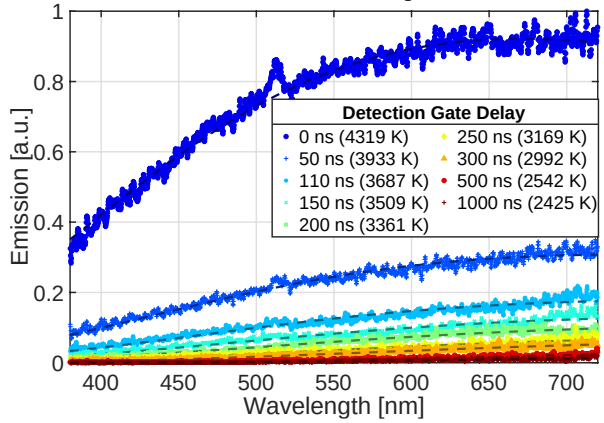

Figure 7: Emission spectra of laser-induced emission for soot particles for different gate delays τ_d for fluence F = 0.3 J/cm^2. The temperature inside the parenthesis is fitted using Eq. (6), with constant $E(m_\lambda) = 0.4$. All curves are normalized by the maximum value obtained at zero gate delay (τ_d = 0).

3.2 Laser-induced emission behavior of dispersed TiO_2 nanoparticle aerosol irradiated at 355 nm

The same strategy used previously for soot particles is applied to characterize the laser-induced emission of dispersed TiO_2 nanoparticles as a function of the laser fluence and detection gate delays to verify (or not) its LII nature.

Figure 8 shows the emission spectra of laser-induced emission of TiO_2 nanoparticles for different laser fluences with a delay of 50 ns to avoid unwanted atomic emissions [23,24]. The spectra show monotonic evolution as a function of the wavelength and are shifted with the laser fluence toward small wavelengths.

This shift can be interpreted regarding the LII theory as a temperature increases for a higher fluence so that the peak of the spectra is blue shifted. The change of peak position between spectra is not as noticeable as in Fig. 6 for soot particles. This may be due to the fact that TiO_2 nanoparticles are characterized by a small absorption function $E(m_{\lambda_{ex}})$. Therefore, during the particle heating process, the laser is hardly absorbed so that the particle temperature is hardly increased and implies a moderate evolution of the emission spectra. The temperature fitting is here not conducted since $E(m_{\lambda_{em}})$ for TiO_2 is nearly zero in 400 – 700 nm (Fig.1).

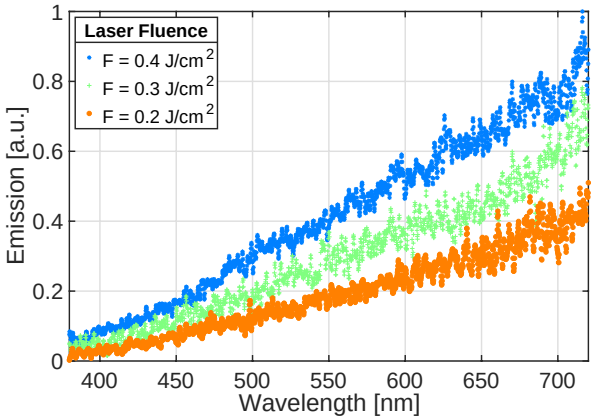

Figure 8: Emission spectra of laser-induced emissions of TiO_2 nanoparticles at various fluences for τ_d=50 ns. All curves are normalized by the maximum value obtained for fluence F = 0.4 J/cm^2.

Figure 9 shows the laser-induced emission spectra of TiO_2 nanoparticles for various gate delays τ_d for a laser fluence F = 0.3 J/cm^2. From the prompt signal (τ_d= 0 ns), it is possible to observe the atomic Ti signal from the sharp peaks close to 500 nm. The peak is not present for τ_d>50 ns, as observed in [23,24]. By increasing the gate delay τ_d, the spectra move towards longer wavelengths. Again, this trend is in agreement with the LII-like nature of the laser-induced emission of TiO_2 nanoparticles.

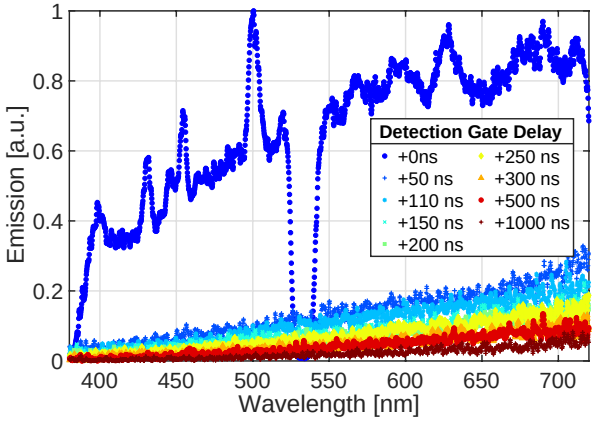

Figure 9: Emission spectra of laser-induced emission of TiO_2 nanoparticles for different τ_d at F=0.3 J/cm2. All curves are normalized by the value at 700 nm obtained at prompt.

Conclusions

In the context of flame-synthesis of nanoparticle production, the laser diagnostics for soot may be generalized to non-carbonaceous particles to improve our knowledge in nanoparticles flame synthesis.

The goal of this work-in-progress study was to verify the feasibility of laser-induced incandescence measurements on engineered TiO_2 nanoparticles aerosol. First, the experimental system was validated with conventional flame-generated soot particles by verifying that the emission spectra follow the black-body radiation behavior. Then, the LII feasibility on TiO_2 nanoparticles was verified using a particle dispersion system at ambient non-reacting conditions to avoid not only the interferences from flame-generated emission but also the possible formation of a carbonaceous layer on the particles or matrix effect with a sampling glass filter. The measurements show that the titanium dioxide nanoparticles can present the black-body-like radiation response to different laser fluences and different gating delays despite the difficulties in excitation and detection of LII measurements from small absorption function $E(m_\lambda)$ in the visible range for TiO_2. On the other hand, at the prompt, unwanted atomic emissions are observed for high laser fluences. It is possible to avoid these non-incandescent emissions by applying lower fluence or delayed detection, as suggested in [23].

Future works will expand the same LII system into flame-synthesized TiO_2 nanoparticles. The feasibility of LII on TiO_2 nanoparticles in flames will address the in situ particle sizing during their formation. Based on the volume fraction and size distribution information under the influence of flame configuration, the chemical and physical mechanisms governing the formation of TiO_2 nanoparticles can be deeply understood for further industrial purposes.

Acknowledgments

This project has received the European Research Council (ERC) support under the European Union's Horizon 2020 research and innovation program (grant agreement No. 757912).

References

[1] M.S. Wooldridge, Prog. Energy Combust. Sci. 24 (1998) 63–87.

[2] S.E. Pratsinis, Fuel Energy Abstr. 39 (1998) 384.

[3] B. Quay, T.W. Lee, T. Ni, R.J. Santoro, Combust. Flame 97 (1994) 384–392.

[4] R.W. Weeks, W.W. Duley, J. Appl. Phys. 45 (1974) 4661–4662.

[5] I.S. Altman, D. Lee, J.D. Chung, J. Song, M. Choi, Phys. Rev. B - Condens. Matter Mater. Phys. 63 (2001) 1–4.

[6] S. Maffi, F. Cignoli, C. Bellomunno, S. De Iuliis, G. Zizak, Spectrochim. Acta - Part B At. Spectrosc. 63 (2008) 202–209.

[7] T.C. Bond, R.W. Bergstrom, Aerosol Sci. Technol. 40 (2006) 27–67.

[8] X. Rocquefelte, F. Goubin, H.J. Koo, M.H. Whangbo, S. Jobic, Inorg. Chem. 43 (2004) 2246–2251.

[9] P. Desgroux, X. Mercier, K.A. Thomson, Proc. Combust. Inst. 34 (2013) 1713–1738.

[10] H.A. Michelsen, J. Chem. Phys. 118 (2003) 7012–7045.

[11] A. Eremin, E. Gurentsov, E. Popova, K. Priemchenko, Appl. Phys. B Lasers Opt. 104 (2011) 285–295.

[12] K. Möls, L. Aarik, H. Mändar, A. Kasikov, A. Niilisk, R. Rammula, J. Aarik, Opt. Mater. (Amst). 96 (2019) 109335.

[13] J. Rams, A. Tejeda, J.M. Cabrera, J. Appl. Phys. 82 (1997) 994–997.

[14] Z.G. Habib, P. Vervisch, Combust. Sci. Technol. 59 (1988) 261–274.

[15] H. Chang, T.T. Charalampopoulos, Proc. R. Soc. London. Ser. A Math. Phys. Sci. 430 (1990) 577–591.

[16] H.A. Michelsen, F. Liu, B.F. Kock, H. Bladh, A. Boiarciuc, M. Charwath, T. Dreier, R. Hadef, M. Hofmann, J. Reimann, S. Will, P.E. Bengtsson, H. Bockhorn, F. Foucher, K.P. Geigle, C. Mounaïm-Rousselle, C. Schulz, R. Stirn, B. Tribalet, R. Suntz, Appl. Phys. B Lasers Opt. 87 (2007) 503–521.

[17] T. Siefke, S. Kroker, K. Pfeiffer, O. Puffky, K. Dietrich, D. Franta, I. Ohlídal, A. Szeghalmi, E.B. Kley, A. Tünnermann, Adv. Opt. Mater. 4 (2016) 1780–1786.

[18] H.Y. Liu, Y.L. Hsu, H.Y. Su, R.C. Huang, F.Y. Hou, G.C. Tu, W.H. Liu, IEEE Sens. J. 18 (2018) 4022–4029.

[19] S. Sarkar, V. Gupta, M. Kumar, J. Schubert, P.T. Probst, J. Joseph, T.A.F. König, ACS Appl. Mater. Interfaces 11 (2019) 13752–13760.

[20] A.C. Eckbreth, J. Appl. Phys. 48 (1977) 4473–4479.

[21] R.L. Vander Wal, T.M. Ticich, J.R. West, Appl. Opt. 38 (1999) 5867.

[22] F. Cignoli, C. Bellomunno, S. Maffi, G. Zizak, Appl. Phys. B Lasers Opt. 96 (2009) 593–599.

[23] S. De Iuliis, F. Migliorini, R. Dondè, Appl. Phys. B Lasers Opt. 125 (2019) 1–11.

[24] Y. Ren, K. Ran, S. Kruse, J. Mayer, H. Pitsch, Proc. Combust. Inst. 000 (2020) 1–9.

[25] M. Hofmann, B.F. Kock, C. Schulz, CEUR Workshop Proc. 211 (2006) 26.

[26] F. Liu, M. Yang, F.A. Hill, D.R. Snelling, G.J. Smallwood, Appl. Phys. B Lasers Opt. 83 (2006) 383–395.

[27] C.S. McEnally, A.M. Schaffer, M.B. Long, L.D. Pfefferle, M.D. Smooke, M.B. Colket, R.J. Hall, Symp. Combust. 27 (1998) 1497–1505.

[28] W.Y. Teoh, R. Amal, L. Mädler, Nanoscale 2 (2010) 1324–1347.